ELSEVIER

International Journal of Mass Spectrometry 206 (2001) 201–210

International Journal of Mass Spectrometry

Reducing grid dispersion of ions in orthogonal acceleration time-of-flight mass spectrometry: advantage of grids with rectangular repeat cells

David S. Selby, Victor Mlynski, Michael Guilhaus*

School of Chemistry, The University of New South Wales, Sydney 2052, Australia

Received 23 February 2000; accepted 27 July 2000

Abstract

In orthogonal acceleration time-of-flight mass spectrometers (oa-TOFMSs), where ion velocity in the axis of the ion source is preserved, the ions approach grids at an angle not equal to 90°. In this situation ions are expected to be dispersed more than in the case of the normal approach. This may be attributed primarily to the effect of grid wires that are not parallel with the source axis. The dispersion leads to a broadening of the flight-time distribution for ions of a given mass-to-charge ratio and hence it degrades mass resolving power. A novel 20 kV matrix-assisted laser desorption/ionisation (MALDI) oa-TOFMS instrument has been used in this study to investigate grid dispersion. The results show that the dispersions that ions experience as they pass through grids/meshes that divide regions of different electric field strength have a significant effect on the resolving power when the majority of the wires are not aligned with the source. Numerical simulations of ion motion point to an advantage in using ideal parallel wire grids with line densities in excess of one hundred lines per centimeter, orientated with the ion source axis. The orientation of parallel wire grids has previously been predicted to significantly affect resolving power in oa-TOF instruments. This article presents the first experimental data to demonstrate the effect. Parallel wire grids of such high line densities are impractical to construct and support so a grid design that approximates parallel wires has been lithographically mastered for electroforming 70% transmission grids with 120 lines per centimeter in one direction and 12 lines per centimeter at right angles to this direction. A resolution loss of ~40% (from a resolution of $m/\Delta m = \sim 8000$ at full width at half maximum) was observed when a three-grid orthogonal accelerator constructed with this material was rotated through 90° from the predicted ideal orientation. The observed linewidths were in reasonable agreement with those predicted by ion trajectory calculations. (Int J Mass Spectrom 206 (2001) 201–210) © 2001 Elsevier Science B.V.

Keywords: Time-of-flight mass spectrometry; Orthogonal acceleration; Ion optics; Mass resolution; Grids

1. Introduction

Grids are used to define boundaries of uniform electric field regions in time-of-flight (TOF) mass spectrometers. They are usually comprised of planar arrangements of wires or other conductive material to which a constant electrical potential is applied [1,2]. Grids are usually substantially transparent to the incident ions with typical transmissions of greater than 50%. Increasing the size of the gaps between the wires increases transmission but allows more field penetration. The curved equipotentials resulting from field penetration (see Fig. 1(a)) have a lens effect that

* Corresponding author. E-mail: m.guilhaus@unsw.edu.au

PII S1387-3806(00)00316-X

causes convergence or divergence of trajectories after they have passed through a gap in the grid. Even when the ions converge, their paths ultimately cross whereupon they become divergent. The net dispersion of ion trajectories caused by this is a source of velocity spread in the TOF direction. This can bring about a measurable increase in the widths of the peaks in the TOF mass spectrum [3].

Bergmann has used analytical calculations to predict the effect of ion dispersion near idealized grids in ion mirrors where the ions approach the grids at right angles [4]. During the development of our orthogonal acceleration time of flight mass spectrometer (oa-TOFMS) systems, [5–8], numerical simulations have indicated a systematic increase in the amount of deflection as, (1) the ratio of the fields separated by the grid increases, (2) the gap between conductors of the grid increases allowing greater field penetration, and (3) the angle of incidence to "wires" that are orientated at right angles to the continuous ion beam deviates from 90° [3,9]. Similar conclusions have been described by others developing oa-TOF instruments [10]. It is noteworthy that in oa-TOF instruments it is highly desirable that the velocity of the ions in the source axis is preserved [9,11] and this requires that the ions approach the grid planes at angles not equal to 90°. Gridless accelerators and ion mirrors are generally not suitable for oa-TOFMS systems because they require that ions remain tightly located near the axis of ion optics where the fields are optimised for correct focusing. It is usual that in oa-TOFMS the ions contained in a few centimeters of the ion beam from the source are accelerated orthogonally into the TOF mass analyzer. Thus the condition of proximity to the axis cannot be met unless very large analyzer dimensions are chosen.

The field differences around grids are optimized to suit the optical design of the spectrometer and these are generally not adjusted to reduce grid dispersion. To do so would in most cases compromise the focusing specifications of the instrument.

The size of the gaps between wires can be greatly reduced by lithographically mastering the grids for production by electrodeposition or etching. Such grids are typically only a few micrometers thick and have a "square-mesh" pattern with regular and equal line densities up to hundreds of lines per centimeter (lpc) in both directions. The first oa-TOFMS instrument developed at UNSW used line spacings of up to 400 lpc to achieve a resolution of about 4000 full width at half maximum (FWHM) for a 1.5 m linear TOF system [5,6]. Unfortunately such grids have the disadvantage of low transmissions ($<$60%) and further reduced transmissions as the angle of incidence deviates from 90°, if the grid thickness is significant on the scale of the distance between wires.

As pointed out by Laiko and Dodonov, when a grid consists of wires that are all parallel to the continuous ion beam in an oa-TOF mass spectrometer, the angle of incidence effect is eliminated [10]. Since the angle of incidence of ions to grids is far from 90° in a typical oa-TOF instrument (especially true for the early grids of the accelerator), the use of parallel wire grids would appear to offer an important advantage. However, relatively high line densities are still required to reduce field penetration.

Due to the practical limitations of constructing parallel wire grids with high line densities, an alternative grid has been designed for this study. It was lithographically mastered and electroformed to have wires running parallel to the source axis spaced at 120 lpc. Crossing wires at right angles to the source axis were spaced at 12 lpc. Relatively few ions passing through such grids should be affected by the 12 lpc wires. Thus the assembly is expected to behave approximately like closely spaced parallel wires.

This article presents a detailed account of observations and calculations with the new grid geometry, extending a recent brief report [12]. In particular, experimentally measured changes in peak width that may be attributed to ion dispersing effects of the grids are presented and discussed. The results have been obtained with a novel oa-TOFMS with a matrix-assisted laser desorption/ionization (MALDI) source. The results should apply to oa-TOFMS systems employing other sources because of the decoupling of source and mass analyzer velocity spreads that is a feature of this instrument geometry [9].

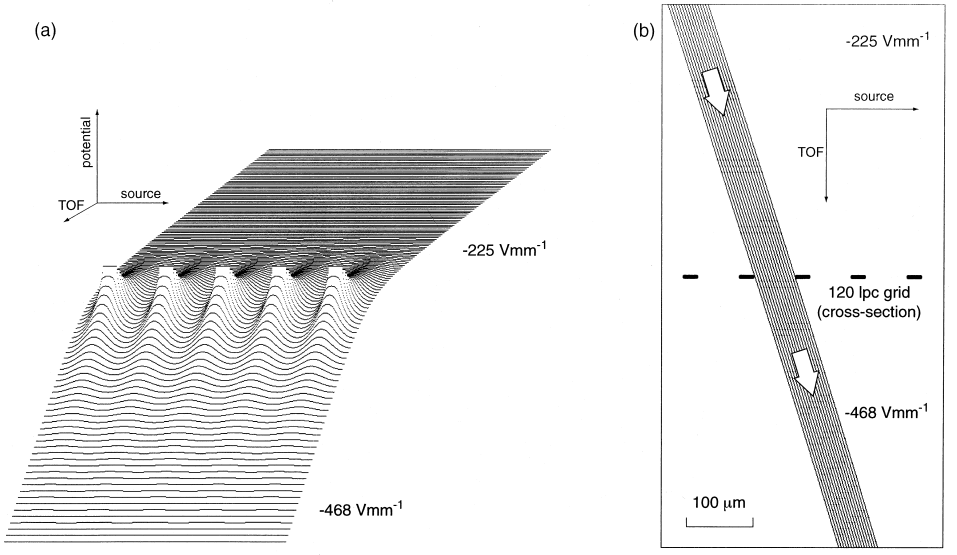

Fig. 1. Simulation of trajectories in the vicinity of grid 2 of the orthogonal accelerator used in this work. The wire cross sections are based on those of the rectangular-mesh grids whereas the simulation models an infinite series of parallel wires spaced at 120 lines per centimeter. Part of the potential function viewed as a surface is shown in (a); the corresponding two-dimensional layout of wire cross sections is shown in (b) with calculated trajectories filling a gap between two of the wires. The slight convergence of ions after passing through the grid is not obvious in the diagram but the calculated final velocities predict substantial temporal spreads arise from this source. Adjacent elements of the potential array represent points in space separated by 1.0 μm.

2. Experiment

2.1. Mass spectrometer

The mass spectrometer used in this work is a custom built oa-TOFMS system with a MALDI source. The TOF analyzer, whose design will be reported in a separate publication, operates with a drift energy of ~20 kV and features a single stage ion mirror separating relatively short drift regions contained in a chamber ~90 cm long and 35 cm wide. The instrument is currently capable of mass analysis of ions up to *m/z* 20 000 in the reflected geometry mode. The instrument does not operate on the principle of delayed extraction and it routinely provides a resolution of ~8000 (FWHM). The salient ion source and TOF mass analyzer parameters are given in Table 1.

2.2. Orthogonal accelerator assembly and alignment

The orthogonal accelerator consists of a push-out plate and three grids supported on grooved rods, fabricated from polyetheretherketone (PEEK, ICI Advanced Materials, Exton, PA, USA). The whole assembly mounts on a stage that simultaneously supports the 70 mm diameter microsphere plate (El-Mul Technologies, Yavne 81104, Israel) reflecting-mode detector assembly. The oa, and the detector are self-aligning to the face of the stage to ensure that all elements are parallel. Likewise the stage registers on the precision machined outer face of the rectangular, solid aluminium chamber to provide correct alignment with the drift region and ion mirror. Three screws allow the entire orthogonal accelerator assembly to be removed, rotated through 90° and reattached to the stage. Fig. 2 shows the construction of orthogonal accelerator.

2.3. Customised 120 lpc × 12 lpc grid material

The electroformed Ni grids were produced according to pattern shown in Fig. 3. A micrograph of this material has been published elsewhere [12]. The grids, which are ~10 μm thick, were attached to the

Table 1
Ion source and mass analyzer parameters for the UNSW 20kV MALDI oa-TOFMS

Source	
Laser	337 nm LSI nitrogen laser
Distance target to oa axis	75 mm
Aperture	2 mm wide at 25 mm from target preceded by lens
Probe Bias	0–200 V
Orthogonal accelerator	
Pushout pulse delay	3–200 μs programmable relative to laser firing
Pushout pulse amplitude	1005 V (60 ns rise time)
1st gap	5.35 mm ($E = -186$ V/mm)
Axis of ion source	1.25 mm from pushout plate
2nd gap	5.50 mm ($E = -225$ V/mm)
3rd gap	40.0 mm ($E = -468$ V/mm)
All grids	12 lpc × 120 lpc, 70% transmission each (normal approach)
Forward drift length	550 mm
Single stage ion mirror	158 mm ($E = 135$ V/mm)
Reflected drift length	619 mm
Detector	70 mm (diameter) Micro Sphere Plate[a]
Digitizer	4 GSample/s × 1 GHz DSO[b]

[a] Single thickness plate with measured pulse width 800 ps in customised assembly with anode operating at ground potential. Plate supplied by El-Mul Technologies (Yavne 81104, Israel).
[b] LeCroy 9384 with PP094 Adapter (LeCroy Corporation, New York).

support rings of the orthogonal accelerator by a method similar to that reported by Bergmann et al [4]. Great care was taken to ensure that the grids were tensioned evenly and that the grid remained flat after mounting.

2.4. Infinite grid array and calculation of partial kinetic energy spreads

Programs such as SIMION 3D (Scientific Instrument Services, Ringoes, NJ, USA) are of great utility in predicting the motion of ions in mass spectrometers. A similar program (I-OPT), also based on classical finite-difference numerical calculations [13] has been developed in our laboratory to have computational features that are well suited to the development of TOFMS systems. One such feature is the ability to simulate an infinite array of parallel wires in sufficient

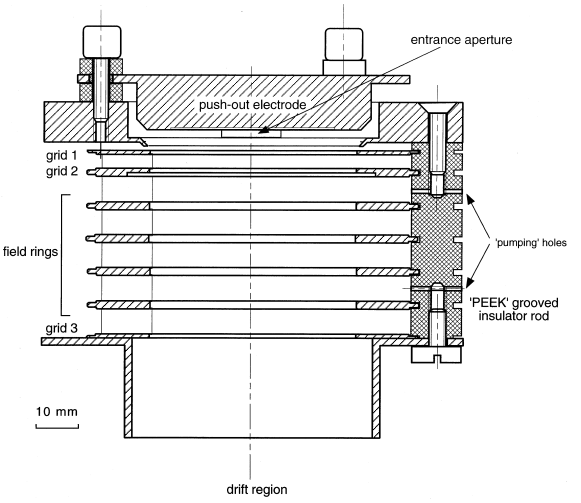

Fig. 2. Cross-sectional view of the orthogonal accelerator used in this work.

detail to model the wire shape and accurately represent the potential function between the wires (see Fig. 1(a)). This is achieved by considering only a small subset of the grid cross section represented in a two-dimensional potential array. The array is made effectively infinite in one axis in the plane of the grid by defining common columns at the boundaries at opposite sides. This may be visualized as though the array is rolled from a plane to form a cylindrical surface as shown in Fig. 4. Thus, in a reasonably

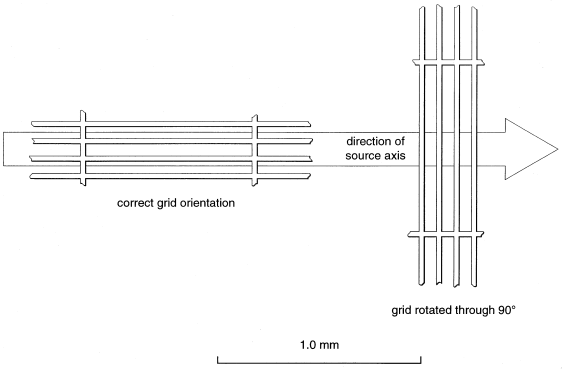

Fig. 3. Scale diagram of small sections of the customized grids showing the correct orientation (left-hand side) with respect to the direction of the ion source axis as well as the rotated orientation (right-hand side) which leads to measurable peak broadening in the TOF mass spectra.

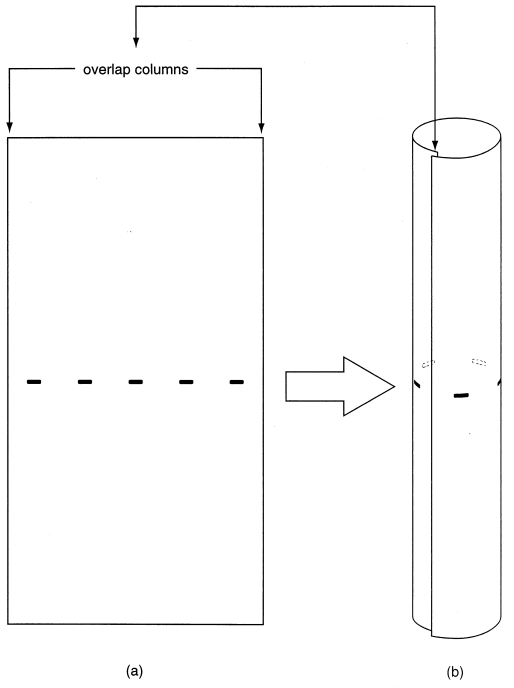

Fig. 4. Schematic representation of the process by which an infinite array of parallel wires is represented in the simulations. The two-dimensional array represented by (a) has its right-most and left-most columns defined to be nonboundary and equivalent. This is conceptually the same as folding the array into a cylinder and overlapping those columns to produce an "infinite" surface (b).

small data array, it is possible to map trajectories accurately at several positions between the wires (see Fig. 1(b)).

Although SIMION 3D was available for this study, the modeling of the grids in three dimensions was not attempted because it was impractical to set up the extremely large array that would have been required to represent the 3D potential function in sufficient detail.

2.5. Transformation of grid-induced dispersion into arrival time spread.

Once the potential function had been calculated for an array as described previously, trajectories were simulated. Ions were given initial velocity components in the direction of the source axis and in the TOF direction. The latter was estimated from the fields experienced by the ions in reaching the boundary of the array. The initial and final velocity components of the ions were compared. For convenience the initial and final velocities were converted to partial kinetic energies (PKEs). In TOF calculations, PKE values, unlike velocity, often have the advantage of being independent of mass. PKE values calculated considering velocity components (u) in a particular direction and multiplying by $+1$ when the velocity is positive and by -1 when it is negative. The ion velocity in the TOF direction is always increasing in an orthogonal accelerator. Changes in velocity in the source direction, on the other hand, remain nearly constant with small changes resulting from field inhomogeneities such as occur around grid wires. Thus any deflection that occurs in a simulated trajectory will be apparent by a change ($\Delta\mathrm{PKE}_{\mathrm{source}}$) in the $\mathrm{PKE}_{\mathrm{source}}$ values between the end and the beginning of the trajectory. It has previously been noted that the PKE lost in the beam axis is gained in the TOF direction and vice versa [3,9]. Thus each $\Delta\mathrm{PKE}_{\mathrm{source}}$ value observed will have a complimentary equal but opposite $\Delta\mathrm{PKE}_{\mathrm{tof}}$ value so that

$$\Delta\mathrm{PKE}_{\mathrm{tof}} = -\Delta\mathrm{PKE}_{\mathrm{source}}. \quad (1)$$

The $\Delta\mathrm{PKE}_{\mathrm{tof}}$ values were then used to calculate the arrival time spread at the detector by assuming ideal fields and drift regions in the remainder of the instrument.

As a check on the quality of the calculation of final velocities and PKE values, I-OPT automatically computes a conservation of energy error factor for each trajectory. Here the final total kinetic energy is calculated in two ways and compared for agreement: (1) the initial kinetic energy (given) and the gain in potential energy (known from the potential array) are added; (2) the kinetic energy based on the mass and final velocity is computed. The latter is based on many steps of numerical integration of the equations of motion. Typical errors of significantly less than 0.01% are obtained in reliable simulations and all results in this article were based on trajectories satisfying this condition.

For a set of trajectories that evenly fills the gap

between two adjacent wires of a grid, there is a corresponding distribution of arrival times. The combined effect of the grids was estimated assuming (1) no correlation and (2) complete correlation. In the uncorrelated case (more likely), the required mathematical convolution of the temporal spreads was performed with commercially available graphing software (IGOR PRO 3.0, Wavemetrics Inc., Lake Oswego, OR, USA).

2.6. MALDI mass spectrometry: samples, matrix, and desorption axis velocity

The mass spectrometer provides a resolving power of at least 8000 FWHM in routine use. Due to the inherent stability of the oa-TOF mass analyzer, the instrument required infrequent external calibration in order to achieve mass accuracies of ~100 ppm. Under these conditions mass accuracy was mainly limited by long-term power supply drift and ion statistics for weak signals.

The matrix used in these experiments was 2,5-dihydroxybenzoic acid (Sigma Chemical Co., St Louis, MO, USA). Samples of 5,10,15,20-tetraphenyl-21H,23H-porphine and gramacidin S analytes were obtained with uncertain origin, but were determined to be pure by mass spectrometry. Bee venom melittin (Sigma), oxidised bovine insulin chain B (Fluka, Chime AG CH-9471, Buchs) and bovine insulin (Sigma) were purchased and also used as analytes. All samples were dissolved in 1:1 (v/v) acetonitrile and 0.5% aqueous trifluoroacetic acid, except for porphine which was dissolved in 1,2-dichloroethane.

Samples were prepared by the dried droplet method, where matrix (10 mg/mL) and analyte (1–4 mg/mL) were sequentially applied to the sample slide, with rapid drying under an infrared lamp between applications. 2 μL of analyte was applied, with a volume of matrix which gave an approximately 1000-fold molar excess of matrix.

Samples were first analyzed in the mass spectrometer with the grids in optimal orientation (see Fig. 3). The grids were rotated through 90° and similar samples were analyzed again. Spectra were obtained across the mass range for which adjacent isotopes were resolved to better than 40% valley. This allowed the estimation of FWHM mass resolution.

Delay times between laser firing and triggering of the push out pulse were varied between 3 and 50 μs across the mass range. This delay is necessary to allow ions to traverse the distance between the MALDI target and the orthogonal accelerator. The ions required an average energy of 205 eV from velocity in the desorption axis in order to reach the centre of the detector after their time-of-fight through the mass analyzer. This relatively high energy was required be in the correct proportion to the ~20 kV orthogonal acceleration potential. Ions entering the orthogonal accelerator with this energy were efficiently transferred to the detector. Some energy was provided by the MALDI process and the rest was given by a bias potential of between 150 and 195 V applied to the sample probe.

3. Results and discussion

3.1. Resolution with optimal and rotated orthogonal accelerator grids

A resolution of 8400 FWHM was obtained at m/z = ~3000 [mellittin, Fig. 5(a)]. The line width was measured at several other masses to construct a relationship to characterize the instrument resolution more thoroughly in Fig. 6(a). In this procedure the square of the peak width was plotted against the mass. This relationship is expected to be linear and it reveals the combined contribution to the peak width of the detector pulse width and timing jitter, evident from the intercept on the ∂t^2 axis [14]. The slope of this graph is a function of the resolution based purely on ion arrival time. Thus an average resolution of ~8000 FWHM was apparent when several experiments over the m/z range ~500–5000 were considered.

The experiments were repeated after rotating the grids of the orthogonal accelerator through 90°. The results are shown in Figs. 5(b) and 6(b) where it is noteworthy that the resolving power (FWHM) for melittin has decreased from 8400 to 4400. The graph revealed a similar overall relative resolution loss for

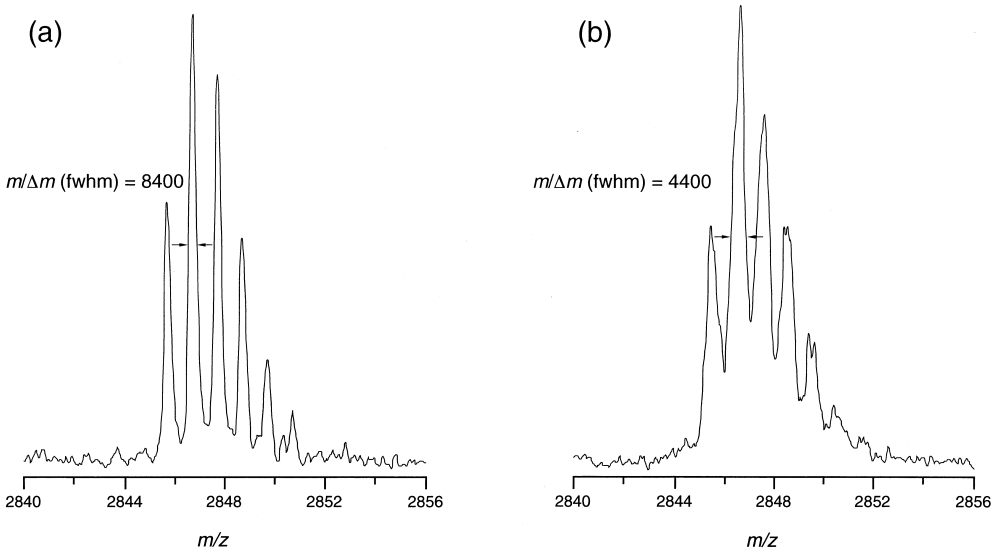

Fig. 5. Molecular ion regions of the MALDI mass spectra of melittin obtained with (a) orthogonal accelerator grids in the correct orientation and (b) in the rotated orientation as defined in the text and in Fig. 3.

the mass range and it also showed that the contribution from detector pulse width and jitter was unchanged and closely matching the value determined from separate direct measurements. Another significant observation in this experiment was that the mass calibration used for the first part of the experiment (grids in optimal orientation) was equally applicable after the rotation of the grids. This is consistent with the energy spread created by the grids being symmetrical around zero.

Finally, the system was restored by rotating the grids to their original orientation. The re-measured resolution values for melittin, gramicidin S and porphine were not significantly different from those measured in the original experiments with grids in the optimal orientation. Again, it was not necessary to recalibrate the mass scale.

3.2. Energy and temporal spreads resulting from ion dispersion at grids

For each grid in the orthogonal accelerator a ΔPKE value was calculated for several ion trajectories generated at regular (2 μm) intervals to fill in the gap between two adjacent wires, as shown in Fig. 1. When the incident angle of trajectories to the grid cross section was set to 90°, the corresponding maximum ΔPKE values were found to be almost negligible for all grids. Values of 0.1, 9.9, and 3.8 meV were obtained for grids 1–3, respectively. This was taken to represent the situation when the grid wires were parallel to the ion source axis.

Much larger ΔPKE values were obtained when the angle of incidence is varied away from 90° as demonstrated when the grids were rotated. ΔPKE_{tof} was sensitive to the angle of approach of ions to the grid, as previously predicted for other grid materials. For a given grid and approach angle, it varied linearly with the position of each trajectory's intersection with the grid plane between adjacent wires [3,9]. The results from these calculations of rotated grids are shown in Fig. 7, where it is apparent that the largest ΔPKE_{tof} occurs with grid 2. It is noteworthy that the magnitude of the slope of the relationship shows the size of the lens effect of the gaps between the wires while the sign indicates if the effect is (initially) converging (positive slope) or diverging (negative slope).

For each grid, the arrival time of the ions at the detector was calculated taking into account the

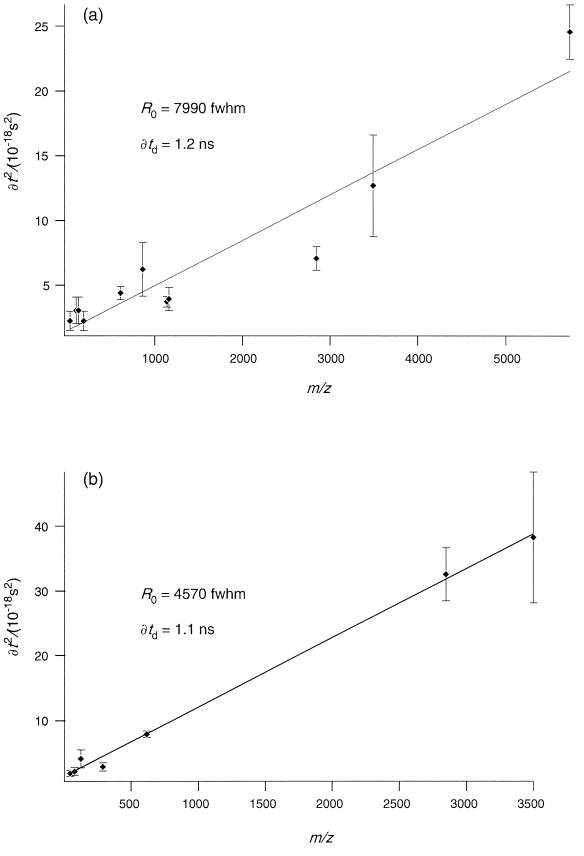

Fig. 6. Variation of peak with (∂t^2) with *m/z* for several masses over a wide mass range for (a) correct and (b) rotated orientations of the orthogonal accelerator grids. The graphs separate the overall instrument resolution (R_0) based on arrival time of ions from the detector pulse width and jitter (∂t_d) as discussed in the text.

ΔPKE_{tof}. The resulting "square" distributions of arrival times are shown in Fig. 8(a).

3.3. Comparison of calculated and measured line widths

The width of the temporal spreads predicted for each of the grids is given in Table 2. The energy spreads from each of the grids would be expected to have a combined effect in the actual instrument. In one model, the combination of these effects would involve little or no correlation. That is, taking the full population of ions, the size and deflection at one grid would be independent of the deflection at the previous

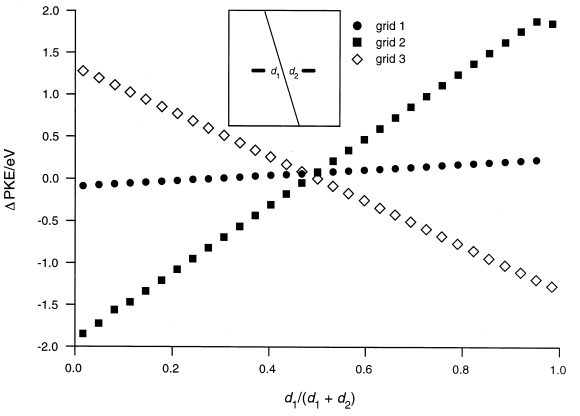

Fig. 7. Changes in partial kinetic energy (ΔPKE) evident from simulations for ions of *m/z* 3000 passing through the each grid of the orthogonal accelerator at regular intervals between adjacent wires as shown in Fig. 1(b). The inset shows how values for the horizontal axis are determined.

grid. The resulting spreads in arrival time should in this case be predicted by convoluting the distributions. In an alternative model there may be some degree of correlation due to the fact that all grids are constructed of the same material and the distance

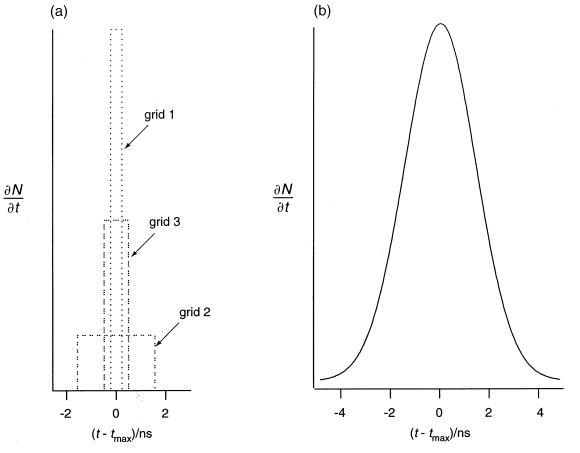

Fig. 8. Temporal distributions (a) calculated from ΔPKE values for a population of *N* ions of *m/z* 3000 passing through the grids in the rotated orientation and (b) of the observed peak shape when the grids are in the correct orientation. In the case of (b), the temporal effects from dispersions at the grids are assumed to be negligible. The observed peak shape with grids in the rotated position should be explained by the combination of the temporal spreads in (a) with the peak shape in (b) as shown in Table 2.

Table 2
Combination of temporal spreads from grids at *m/z* 3000

Source of PKE and Δt	PKE (eV)	Δt (ns)
(1) Observed FWHM 0°		3.46
(2) Observed FWHM 90°[a]		5.79
(3) Calculated individual effect of rotated grids[b]		
Grid 1 (ion approach at average angle of 63°)	0.31	0.47
Grid 2 (ion approach at average angle of 72°)	5.40	3.13
Grid 3 (ion approach at average angle of 84°)	2.56	0.99
(4) Calculated combined effect of rotated grids		
Linear addition		4.59
Convolution		2.40
(5) Grid FWHM required to convolute with (1) to give (2)		3.65

[a] Average FWHM line width predicted in Fig. 6.
[b] ΔPKE and Δt negligible in 0° orientation (see the text).

between them is not great relative to the deflection angles. In one (highly unlikely) specific case of correlation the individual temporal spreads would add constructively. Table 2 combines the calculated temporal distributions by convolution and by simple addition and predicts the ultimate line width expected if there is negligible temporal spread with the grids in the correct orientation. At 2.4 ns the calculated total Δt contribution from grids in the uncorrelated model is 34% lower than required to explain the observed broadening that occurs when the grids are rotated. Not surprisingly, the correlated model overestimates the effect. Since it is unlikely that the grid deflections are highly correlated, a more likely explanation of the discrepancy may be that it arises from a combination of factors. These could include: (1) some degree of constructive correlation in the deflections, (2) the effect of the wires at 12 lpc (not considered in the calculations), and (3) the simplifying assumption that the ions all have the average desorption energy from the MALDI probe. Taking these factors into account the observed and predicted increase in line width resulting from the rotation of the grids is reasonable.

3.4. Rectangular-mesh grids versus square-mesh grids

The issue of trajectory dispersion by parallel wire grids compared to square-mesh grids was first discussed with respect to oa-TOFMS instruments by Laiko and Dodonov who acknowledged that it was difficult to conclude which geometry was superior [10]. These authors predicted the larger "scattering" effect of the wires that are orientated at right angles to the continuous ion beam and our experimental data are apparently the first to support the prediction. A direct comparison between our rectangular-mesh grid (in the optimal orientation) with a 120 lpc × 120 lpc square-mesh grid is not possible with the current configuration of our apparatus. However, we would postulate that the square-mesh grid would have an effect on resolution intermediate between the two configurations compared in our experiment. This is due to the expected influence of the larger number of wires at right angles to the continuous ion beam in the case of the square-mesh grid.

The use of 120 lpc × 120 lpc square-mesh grid would involve a lower transmission than for the rectangular mesh. Transmission would be lower at least by a factor obtained from the ratio of transmissions in the two geometries, raised to the power of the number of grids. For example, for a 120 lpc × 120 lpc square-mesh, with "wire" width the same as in Fig. 3, the transmission for each grid is 55% compared to 70% for the rectangular-mesh grid. Thus for a three grid assembly the "rectangular" set has a total transmission $(0.7/0.55)^3 = 2.1$ times greater than that of the square mesh. This factor becomes even less favorable for the square-mesh grids when their thickness is taken into account for ions that approach them at other than 90°.

4. Conclusion

Predicted dispersions of ions passing through grids that approximate parallel wires have been shown to be in reasonable agreement with experimental results, as evident from peak broadening and associated resolution losses in an oa-TOFMS instrument. The correct alignment of the grids, such that the source axis is aligned with the closely spaced wires is important to minimize the dispersion of ions. These dispersions occur predominantly when ions approach wire cross-

sections at angles that are not very close to 90°. An implication of the results is that the rectangular-mesh grid geometry potentially offers better resolution and transmission characteristics when used in oa-TOFMS instruments, when compared to the conventional square-mesh grids.

Acknowledgements

The continued financial support of the Australian Research Council is gratefully acknowledged. The authors thank Dr. J.J. Brophy and Dr. K. Fisher for generously providing samples of gramacidin S and tetraphenylporphine, respectively.

References

[1] R.J. Cotter, Time-of-Flight Mass Spectrometry: Instrumentation and Applications in Biological Research, American Chemical Society, Washington, DC, 1997, p. 326.
[2] M. Guilhaus, J. Mass Spectrom. 30 (1995) 1519.
[3] M. Guilhaus, V. Mlynski, D. Selby, Rapid Commun. Mass Spectrom. 11 (1997) 951.
[4] T. Bergmann, T.P. Martin, H. Schaber, Rev. Sci. Instrum. 61 (1990) 2592.
[5] J.H.J. Dawson, M. Guilhaus, Rapid Commun. Mass Spectrom. 3 (1989) 155.
[6] J. Coles, M. Guilhaus, Trends Anal. Chem. 12 (1993) 203.
[7] M. Guilhaus, M. Stutsel, J. Coles, in Proceedings of the 42nd ASMS Conference on Mass Spectrometry and Allied Topics. Chicago, IL, 29 May–3 June 1994, p. 503.
[8] V. Mlynski, M. Guilhaus, Rapid Commun. Mass Spectrom. 10 (1996) 1524.
[9] M. Guilhaus, D. Selby, V. Mlynski, Mass Spectrom. Rev. 19 (2000) 65.
[10] V.V. Laiko, A.F. Dodonov, Rapid Commun. Mass Spectrom. 8 (1994) 720.
[11] M. Guilhaus, J. Am. Soc. Mass Spectrom. 5 (1994) 588.
[12] D.S. Selby, V. Mlynski, M. Guilhaus, Rapid Commun. Mass Spectrom. 14 (2000) 616.
[13] K.J. Bins, P.J. Lawrenson, Analysis and Computation of Electric and Magnetic Field Problems, Pergamon, Oxford, 1963, p. 333.
[14] J.N. Coles, M. Guilhaus, J. Am. Soc. Mass Spectrom. 5 (1994) 772.